Synthesis of Poly(methylmethacrylate-co-butylacrylate) Nanocompounds and Silver Nanoparticles Using Sustainable Method.

P.F. Vera-García[a], L. Farías-Cepeda[a], S. Vázquez-Rodríguez[b], P. Acuña-Vazquez[c], R. Díaz de León[c], A. Sáenz Galindo[a], A. O. Castañeda-Facio[a]*

[a]Facultad de Ciencias Químicas. Universidad Autónoma de Coahuila, Blvd. Venustiano Carranza esq. José Cárdenas Valdés Col. República CP. 25280 1, Saltillo, Coahuila, México.

[b]Facultad de Ingeniería Mecánica y Eléctrica. Universidad Autónoma de Nuevo León, Pedro de Alba SN, Niños Héroes, Ciudad Universitaria, CP 66451, San Nicolás de los Garza, Nuevo León, México.

[c]Centro de Investigaciones en Quimica Aplicada, Enrique Reyna H. 140, San José de los Cerritos, Saltillo, Coahuila, 25294, México

Síntesis de Nanocompuestos de Poli(metilmetacrilato-co-butilacrilato) y Nanopartículas de Plata Mediante Métodos Sustentables

Síntesi de Nanocompostos de Poli(metilmetacrilat-co-butilacrilat) i Nanopartícules de Plata Mitjançant Mètodes Sustentables

RECEIVED: 23 JUNE 2022; ACCEPTED: 13 SEPTEMBER 2023; HTTPS://DOI.ORG/XXX

ABSTRACT

Nanocomposites of poly(methylmethacrylate-co-butylacrylate) P(MMA-co-BuA) and silver nanoparticles (NPsAg) synthesized with extracts of *O. ficus-indica* (OFI) and *A. vera* (AV) were obtained by using microwaves. The nanocomposites were synthesized by "*in situ*" emulsion polymerization, where different concentrations of NPsAg (0.05, 0.1, 0.5 and 1%) with respect to the polymer were studied. Films were formed from the latex, which were characterized by different techniques. Using UV-Vis, the characteristic absorbance of the surface plasmon resonance of the NPsAg in the nanocomposite was observed in the range of 415-436 nm. The thermal stability of the nanocomposites was carried out using TGA, where it was observed that the higher the concentration of NPsAg, the lower the thermal stability. The DSC results showed that the glass transition temperatures (Tg) for the nanocomposites with nanoparticles are between 8 and 12°C. The percentage elongation of the nanocomposites was 400%, in addition, the Young's modulus and the tensile strength of the same were determined, observing that the higher the content of NPsAg, the lower the elastic behavior and the mechanical resistance of the nanocomposites. Using SEM, it was confirmed that the NPsAg maintain a spherical morphology. Finally, using FTIR, the possible interaction between the PMMA-Co-BuA copolymer and the NPsAg was determined.

Keywords: P(MMA-co-BuA), emulsion polymerization, silver nanoparticles.

RESUMEN

Se obtuvieron nanocompuestos de poli (metilmetacrilato-co-butilacrilato) P(MMA-co-BuA) y nanopartículas de plata (NPsAg) sintetizadas con extractos de *O. ficus-indica* (OFI) y *A. vera* (AV) mediante el uso de microondas. Los nanocompuestos se sintetizaron mediante polimerización en emulsión "*in situ*", donde se estudiaron diferentes concentraciones de NPsAg (0.05, 0.1, 0.5 y 1%) respecto al polímero. A partir del látex se formaron películas, las cuales se caracterizaron por diferentes técnicas. Mediante UV-Vis se observó en el

***Corresponding author: adali.castaneda@uadec.edu.mx**

rango de 415-436 nm la absorbancia característica de la resonancia del plasmón superficial de las NPsAg en el nanocompuesto. La estabilidad térmica de los nanocompuestos se realizó mediante TGA, donde se observó que a mayor concentración de NPsAg la estabilidad térmica es menor. Los resultados de DSC mostraron que las temperaturas de transición vítrea (Tg) para los nanocompuestos con nanopartículas están entre 8 y 12°C. El % de elongación de los nanocompuestos fue de 400%, además se determinó el módulo de Young y la resistencia tensil de los mismos, observando que a mayor contenido de NPsAg el comportamiento elástico y la resistencia mecánica de los nanocompuestos disminuyen. Mediante SEM se confirmó que las NPsAg mantienen una morfología esférica. Finalmente, por FTIR se determinó la posible interacción entre el copolímero P(MMA-co-BuA) y las NPsAg.

Palabras clave: P(MMA-co-BuA), polimerización en emulsión, nanopartículas de plata.

RESUM:

Es van obtenir nanocompostos de poli(metilmetacrilat-co-butilacrilat) P(MMA-co-BuA) i nanopartícules de plata (NPsAg) sintetitzades amb extractes d'O. ficus-indica (OFI) i A. vera (AV) mitjançant l'ús de microones. Els nanocompostos es van sintetitzar mitjançant polimerització en emulsió "in situ", on es van estudiar diferents concentracions de NPsAg (0.05, 0.1, 0.5 i 1%) respecte al polímer. A partir del làtex es van formar pel·lícules, les quals es van caracteritzar per diferents tècniques. Mitjançant UV-Vis es va observar en el rang de 415-436 nm l'absorbància característica de la ressonància del plasmó superficial de les NPsAg al nanocompost. L'estabilitat tèrmica dels nanocompostos es va realitzar mitjançant TGA, on es va observar que com més concentració de NPsAg l'estabilitat tèrmica és menor. Els resultats de DSC van mostrar que les temperatures de transició vítria (Tg) per als nanocompostos amb nanopartícules estan entre 8 i 12 . El % d'elongació dels nanocompostos va ser de 400%, a més a més es va determinar el mòdul de Young i la resistència tensil dels mateixos, observant que com més contingut de NPsAg el comportament elàstic i la resistència mecànica dels nanocompostos disminueixen. Mitjançant SEM es va confirmar que les NPsAg mantenen una morfologia esfèrica. Finalment, per FTIR es va determinar la possible interacció entre el copolímer P(MMA-co-BuA) i les NPsAg.

Paraules clau: P(MMA-co-BuA), polimerització en emulsió, nanopartícules de plata

INTRODUCTION

Currently, the use of nanoparticles for the development of composite materials has become a focus of growing attention due to its applications in different areas such as pharmacy, medicine, biology, agriculture, among others. The incorporation of noble metal nanoparticles specifically those of Ag with particle sizes between 2-100 nm imparts very interesting properties to composite materials mainly due to their size and morphology. To obtain these properties, it is essential to control the size distribution, dispersion and morphology of the nanoparticles, as well as the concentration of some polymer matrix. Nanoparticles can modify the mechanical, electrical, optical and magnetic properties of the polymeric matrix in which they are found; hence the great boom that nanoscience and nanotechnology currently have in various areas, all always aimed at improving the quality of life of human beings [1–10].

There are different ways of preparing a nanocomposite, such as melt mixing [11,12], solution mixing [13] and *in situ* polymerization [14,15]. In *in situ* polymerizations, polymerization is carried out in the presence of the nanoparticles, either in homogeneous or heterogeneous systems. Among the heterogeneous polymerization techniques, emulsion polymerization stands out to obtain a composite latex and subsequently a nanocomposite [16–18]. Emulsion polymerization is used industrially for the manufacture of paints, coatings, adhesives, paper coatings and carpet backings. Polyacrylates (PA) are one of the most used families for water-based coatings and within acrylic emulsions, the most used are methyl methacrylate (MMA) [19] and butyl acrylate (BuA) [20]. Emulsion polymerizations are carried out via free radicals, which begins as an oil-type emulsion (monomer) in water [21] and ends as a colloidal dispersion of particles (latex). In the process, surfactants that have the function of forming and stabilizing the polymeric particles are used; in addition, an initiator is used to generate free radicals. Nanocomposites obtained from composite latex present better properties, attributed mainly to the properties that nanoparticles provide when incorporated into latex [17,22–30].

Currently, various scientific studies are focused on the analysis of composite materials based on a polymeric matrix and metallic nanostructures or nanoparticles such as the inorganic phase, as mentioned by Mamaghani et al. [31] where they synthesized a nanocomposite based on methylmethacrylate-butylacrylate-acid acrylic with NPsAg using two methodologies, the first was by mixing nanoparticles in the latex and the second methodology was by polymerization in mini emulsion *in situ* in the presence of the nanoparticles. They mention that the *in situ* methodology of the nanocomposite had the best results, showing an increase in the degradation temperature and in the glass transition temperature, improving thermal stability compared to the pure copolymer, attributing it to the good interaction and interfacial compatibility of the polymer and silver nanoparticles. On the other hand, Abdelaziz et al. [32] studied the thermal properties of the poly(methyl methacrylate) thin (PMMA) and $AgNO_3$ nanocomposite obtained by mixing in solution and the films by evaporating the solvent and varying the concentration of the nanoparticles from 0-10%, they found that the thermal stability of the nanocomposites decreases with increasing concentration of Ag. Alghunaim et al. [19] synthesized nanocomposites based on poly(methyl

methacrylate) and polycarbonate PMMA/PC with copper oxide nanoparticles (NPsCuO) in different concentrations 0, 0.25, 0.50 and 0.75% by melt mixing. They studied the dielectric properties of the nanocomposites, observing that elongation at break (ε) values gradually increased with a higher content of nanoparticles compared to the pure polymer, attributed to the high values of the dielectric permittivity of NPsCuO. This research work aims to evaluate the thermal and mechanical properties of P(MMA-co-BuA) and NPsAg nanocomposites obtained from composite latex. The composite latexes were synthesized by *in situ* emulsion polymerization of MMA and BuA in the presence of silver nanoparticles which were synthesized in the presence of plant extracts of OFI and AV. It is important to mention that the synthesis of nanoparticles with these extracts is mainly due to obtaining nanoparticles with green methodologies that do not involve toxic reagents. On the other hand, these desert plants are very abundant in our region (Saltillo Coahuila, México), being a low-cost local resource. In this study it is intended to use the plant extracts as reducing and stabilizing agents, since they are plants rich in polyphenols. Until now, few publications have been found where the extracts of OFI and AV are used as reducing and stabilizing agents for the synthesis of silver nanoparticles. Likewise, no reports have been found where nanoparticles obtained by biosynthesis are incorporated by emulsion polymerization *in situ* to the P(MMA-Co-BuA) copolymer to obtain a nanocomposite, presenting an area of opportunity for its study and glimpsing an aspect to promote sustainable methodologies with lower environmental impact.

MATERIALS AND METHODS

1.1 Material

NPsAg were synthesized from plant extracts OFI and AV by means of microwaves, the synthesis of which has been previously reported by Vera-García et al. [33]. Monomers MMA (99%) and BuA (99%) were purchased from Aldrich. The sodium hydroxide with which the monomer inhibitor was removed (NaOH, 98%) was purchased from Jalmek, the surfactant, sodium dodecyl sulfate (SDS, 98%) was purchased from Jalmek and the initiator, ammonium persulfate ($(NH_4)_2S_2O_8$, 98%) was purchased from Jalmek.

1.2 Emulsion polymerization of MMA and BuA in the presence of NPsAg

First, the MMA and BuA monomers were washed with a 10% NaOH solution, the monomer and the NaOH solution were added in a separatory funnel, stirred and left to stand for 2 min. Subsequently, the monomer was collected to carry out two more washes. Finally, the washing procedure was repeated 3 more times with distilled water and the collected monomer was stored in the refrigerator until use.

The polymerization reactions were carried out in a 100 mL jacketed glass reactor, fitted with a heating bath to control the reaction temperature at 70°C and a mechanical stirrer at 300 rpm was used. During the polymerization reactions, a flow of N_2 was maintained. First, the NPsAg were dispersed in an SDS solution (10 g of water and 0.94 g of SDS) by means of an ultrasound bath for 10 min. Subsequently, this dispersion was placed in the reactor and 0.18 g of $(NH_4)_2S_2O_8$ was added as initiator and 65.5 g of water as dispersant. Stirring and the flow of N_2 were initiated, once the mixture reached the reaction temperature, the monomer mixture was dosed for 30 min, which is composed of 7 g of MMA and 6.2 g of BuA (53% of MMA and 47% BuA), the reaction was left for 4.5 h post-addition. The percentage of nanoparticles was varied with respect to the total monomer. Once the composite latexes had been synthesized, films were made by evaporation of solvent (water), the solution was placed in molds and the solvent was allowed to evaporate for 48 h at 40°C. Table 1 shows the conditions for obtaining the nanocomposites and their identification.

Table 1. *Reaction conditions for P(MMA-co-BuA) / NPsAg nanocomposites.*

Sample name	Extract in which the nanoparticles were obtained	NPsAg %
P(MMA-co-BuA)	*O. ficus-indica*	0
P(MMA-co-BuA)-OFI-0.05%		0.05
P(MMA-co-BuA)-OFI-0.1%		0.1
P(MMA-co-BuA)-OFI-0.5%		0.5
P(MMA-co-BuA)-OFI-1%		1
P(MMA-co-BuA)-AV-0.05%	*A. vera*	0.05
P(MMA-co-BuA)-AV-0.1%		0.1
P(MMA-co-BuA)-AV-0.5%		0.5
P(MMA-co-BuA)-AV-1%		1

2.1 Characterization of P(MMA-co-BuA) and NPsAg nanocomposites

The characterization of the films was carried out using FTIR spectroscopy in a Perkin Elmer Frontier model equipment to observe the functional groups in the nanocomposite, using UV-Vis, the surface plasmon resonance (SPR) of the NPsAg in the nanocomposite was evaluated, this analysis was performed on a Cary 5000 with a coupled integration sphere. The thermal stability of the nanocomposites was carried out by means of TGA in a STA PT 1600 equipment from Linseis, using a heating ramp of 10°C/min from 30°C to 800°C in a nitrogen atmosphere. The Tg of the materials was determined by DSC in a Perkin Elmer Diamond equipment, using a heating rate of 10°C/min, from -20°C to 150°C, under nitrogen flow. The mechanical tests such as Young's modulus, tensile strength (σ) and elongation at break (ε) were carried out in a TA.XT.Plus model uniaxial equipment, under ambient conditions at a tensile speed of 30 mm/min, the dimensions of the specimens were 50 mm x 10 mm, with a thickness of 0.4 mm. Five tests were carried out for each sample and the average of them was taken.

RESULTS AND DISCUSSION

The films obtained are shown in Figure 1, where it can be seen in Figure 1a) the P(MMA-co-BuA) copolymer, in Figure 1b) nanocomposites with NPsAg obtained with the OFI extract and in Figure 1c) the nanocomposites with NPsAg obtained with the AV extract. As can be seen at a higher concentration of silver nanoparticles, the color of the nanocomposite intensifies.

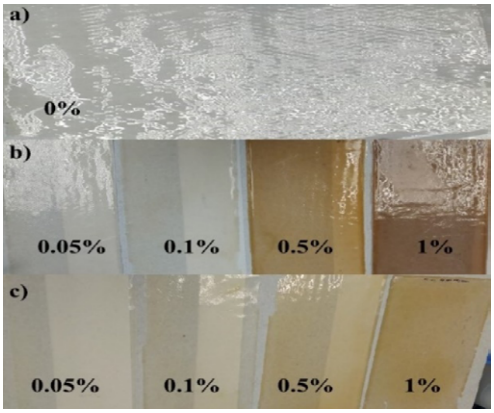

Figure 1. *Films of a) P(MMA-co-BuA) copolymer b) P(MMA-co-BuA) nanocomposite and nanoparticles obtained with OFI extract and c) P(MMA-co-BuA) nanocomposite and nanoparticles obtained with the AV extract.*

3.1 UV-Vis analysis

In Figure 2, the UV-Vis spectra of the nanocomposites are shown, where the surface plasmon resonance (SPR) from the silver nanoparticles can be observed. It should be noted that the SPR occurs when the free electrons in the conduction band of the nanoparticle surface are capable of interacting with electromagnetic radiation in a complex way, having some excitation at a certain wavelength, which will depend on the shape, size and chemical nature of the nanoparticle [34–37]. In Figure 2a, the UV-Vis spectra of P(MMA-co-BuA) and NPsAg nanocomposites are presented, whose nanoparticles were obtained with the OFI extract, the nanocomposites with 0.05 and 0.1% do not present an absorption band because the concentration of NPsAg is very low and the team failed to detect it. However, the 0.5 and 1% nanocomposites present the SPR of Ag in a range of 427-436 nm. In Figure 2b, the UV-Vis spectra of the nanocomposites whose nanoparticles were synthesized from the AV extract are observed. As previously observed, nanocomposites at 0.05 and 0.1% do not present an absorption band and nanocomposites at 0.5 and 1% present plasmon in a range of 415-423 nm, confirming the presence of nanoparticles in the nanocomposite. Deshmukh et al., [38] similarly investigated SPR in PMMA-NPsAg nanocomposites at different concentrations of silver nanoparticles (5, 10 and 20%), obtaining results very similar to those obtained in this work. While Roshmi et al., synthesized PMMA-NPsAg films using solvent casting method, obtaining the SPR of the nanocomposites around 350-470 nm [39].

3.2 TGA analysis

The thermal stability of the nanocomposites with the nanoparticles obtained with OFI and AV extract are shown in Table 2. Observing in general the weight loss of the P(MMA-co-BuA) copolymer that presented three stages, the first weight loss was at approximately 296 °C, corresponding to 2.1% loss of the sample, which is due to removal of unsaturated chains and decomposition of PMMA [32,40]. Then the second loss occurs at around 327 °C, with 16.3% weight loss corresponding to decomposition which corresponds to SDS decomposition [41], and the last drop at 400 °Cwith

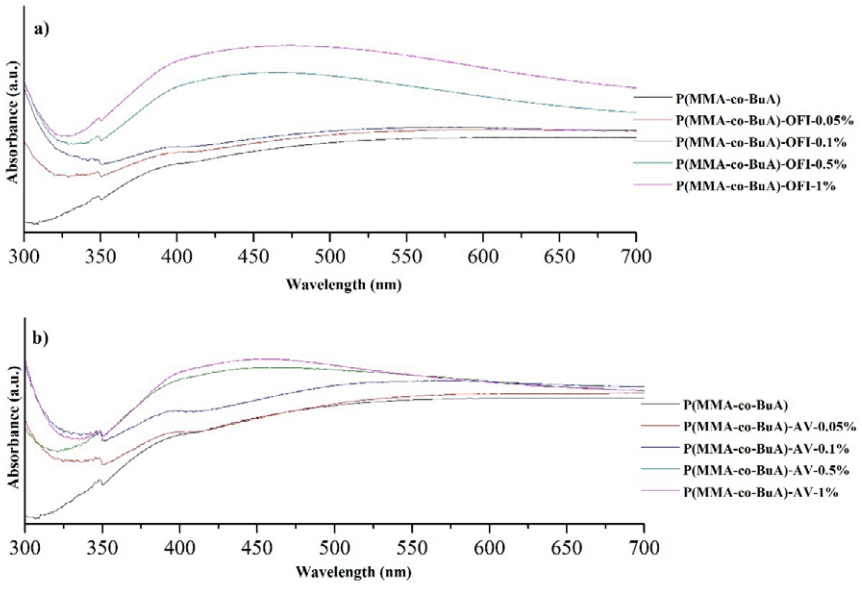

Figure 2. *UV-Vis spectra a) P(MMA-co-BuA) and NPsAg from the OFI extract and b) P(MMA-co-BuA) and NPsAg from the AV extract at different concentrations.*

97.3% total loss of sample, which can be attributed to the degradation of the copolymer chains [3]. Finally at 357 °C the maximum temperature is shown where the greatest loss in weight of the sample occurred. Buhin et al. [3] determined the degradation temperatures of the P(BuA-co-MMA) copolymer (50/50) obtaining similar results since their copolymer presented 3 losses in weight, the first and second in the range of approximately 250-375°C and the third fall at 375-450°C .

Table 2. *Degradation temperature from TGA of the nanocomposites with OFI and AV extracts.*

Compound	Decom-position	Temperature°C	% Losses in weight	T. max °C
P(MMA-co-BuA)	1	296	2.1	357
	2	327	16.3	
	3	400	97.3	
P(MMA-co-BuA)-OFI-0.05%	1	266	9.4	350
	2	336	49.4	
	3	388	94.1	
P(MMA-co-BuA)-OFI-0.1%	1	262	3.4	346
	2	339	43.1	
	3	391	90.15	
P(MMA-co-BuA)-OFI-0.5%	1	264	9.1	348
	2	386	88.5	
P(MMA-co-BuA)-OFI-1%	1	264	2.4	316
	2	385	91.3	
P(MMA-co-BuA)-AV-0.05%	1	255	8.9	335
	2	333	45.1	
	3	385	91.3	
P(MMA-co-BuA)-AV-0.1%	1	278	8.5	323
	2	382	96.5	
P(MMA-co-BuA)-AV-0.5%	1	251	5.8	357
	2	362	29.8	
	3	393	88.3	
P(MMA-co-BuA)-AV-1%	1	282	2.5	319
	2	389	91	

Table 3 shows the temperatures at which 5 and 50% loss of weight of the nanocomposites occurs, where it can be observed that the said temperatures are lower than those of the P(MMA-co-BuA) copolymer compared to the nanocomposites in all cases. This means that when incorporating the NPs, the thermal stability of the nanocomposite decreases at least for the concentrations studied.

Table 3. *Temperatures with respect to weight losses and maximum degradation temperatures of the P(MMA-co-BuA) copolymer and of the P(MMA-co-BuA)/NPsAg nanocomposites from the extracts of OFI and AV.*

Compound	T5% (°C)	T50% (°C)
P(MMA-co-BuA)	313	362
P(MMA-co-BuA) OFI-0.05%	290	348
P(MMA-co-BuA) OFI-0.1%	288	346
P(MMA-co-BuA) OFI-0.5%	186	345
P(MMA-co-BuA) OFI-1%	193	337
P(MMA-co-BuA) AV-0.05%	304	348
P(MMA-co-BuA) AV-0.1%	210	337
P(MMA-co-BuA) AV-0.5%	188	339
P(MMA-co-BuA) AV-1%	193	337

3.3 DSC analysis

The simple way to observe the effect of NPsAg on the copolymer is by analyzing the behavior of the glass transition. Table 4 shows the glass transition temperature (Tg) of the nanocomposites where it can be seen that the P(MMA-co-BuA) copolymer without nanoparticles has a Tg of around 8.9°C and this value increases as the concentration of the nanoparticles increases regardless of the extract with which they were obtained, perhaps this behavior is due to the interaction of hydrogen bridges that are generated between the functional groups of the P(MMA-co-BuA) copolymer with the functional groups of the extracts that are located on the surface of the NPsAg, and consequently, as the content of nanoparticles increases in the nanocomposite, the movement of the chains that are around the nanoparticles is restricted, causing the interfacial interactions to become more considerable with the increase in the concentration of the nanoparticles [42,43], suggesting a strong interaction between the chains of the copolymer and the nanoparticles. It can be observed that with increase in the concentration of NPsAg, the Tg values increase. The P(MMA-co-BuA) AV-1% nanocomposite has a Tg of 9.2°C, in general, nanocomposites with NPsAg from AV extract show a very similar trend, that is, the Tg increases with the content of NPsAg.

Table 4. *Values obtained from glass transition temperatures (Tg) by DSC.*

O. ficus-indica	Tg (°C)	vera	Tg (°C)
P(MMA-co-BuA)	8	P(MMA-co-BuA)	8
P(MMA-co-BuA) OFI-0.05%	9.1	P(MMA-co-BuA) AV-0.05%	7.6
P(MMA-co-BuA) OFI-0.1%	10.7	P(MMA-co-BuA) AV-0.1%	10
P(MMA-co-BuA) OFI-0.5%	12.24	P(MMA-co-BuA) AV-0.5%	9.59
P(MMA-co-BuA) OFI-1%	12.6	P(MMA-co-BuA) AV-1%	9.18

3.4. Mechanical properties

Table 5 shows the results obtained from the stress test of the P(MMA-co-BuA) nanocomposites with and without NPsAg. The percentage elongation at break of the film without nanoparticles shows a deformation of 500%, while the nanocomposite P(MMA-co-BuA) OFI-1% has an elongation value of 400%. The same behavior is exhibited by nanocomposites with nanoparticles synthesized with AV extract; as the concentration of NPsAg increases, the elongation percentage decreases due to the decrease in mechanical resistance and therefore a fracture occurs more quickly [44]. The results of this work agree with those obtained by Ghaffari et al. [24] who found that at high concentrations of NPsAg in the polymer, the mechanical properties tend to decrease, making the nanocomposite more brittle, presenting low fracture energy. The P(MMA-co-BuA) presents a Young's modulus of 98. 5 MPa, while the compounds

P(MMA-co-BuA) OFI-1% and P(MMA-co-BuA) AV-1% presented moduli of 16.1 and 13.1 MPa, respectively. In general, it is observed that as the percentage of NPsAg increases, the elastic behavior decreases. This same behavior was observed by Zhang et al. [45] in PMMA nanocomposites with graphene particles, attributing the decrease in modulus and mechanical resistance to the weak interfacial interaction between the matrix and the reinforcement. At the breaking point of the samples, the tensile strength was calculated, where it can be seen that the white P(MMA-co-BuA) has a tensile strength of 6.6 MPa before fracture, while the P(MMA-co-BuA) OFI-1% sample had a strength of 2.8 MPa. As can be seen in Table 4, the tensile strength of nanocomposites where NPsAg from the *O. ficus-indica* extract was used remains around 2.5-2.9 MPa regardless of the concentration of the NPsAg. The P(MMA-co-BuA) AV-1% sample presented tensile strength of 3.6 MPa, while the remaining nanocomposites obtained similar results at 2 MPa, implying that the increase in the content of NPsAg decreases the mechanical resistance of the material. Morimune et al. [46] and Tripathi et al. [44] obtained similar results for PMMA nanocomposite with graphene oxide, they observed that by increasing the reinforcement in the matrix, the tensile strength decreases since the nanocomposite becomes more fragile due to the presence of oxide agglomerates of graphene. For their part, Monje et al. [47] studied the mechanical and thermal properties of polyurethane nanocomposites with NPsAg, finding that, by incorporating the reinforcement in the polymer, the properties studied decreased. They attributed it to the formation of NPsAg aggregates and to the decrease in the mobility of the polymer chains as NPsAg are present and increased rigidity. Perez-Martinez et al. [15] found a similar behavior for P(MMA-co-BuA) nanocomposites with multiple wall carbon nanotubes (MWCNTs) synthesized by "*in situ*" mini emulsion polymerization and proposed that due to the process "*in situ*", it increases the interaction between the polymer and MWCNTs (graft reactions) that reduce the mobility of the polymer chains.

Table 5. *Values of mechanical properties of tension of the copolymer of P(MMA-co-BuA) and of the nanocomposites P(MMA-co-BuA) and NPsAg.*

Samples	Elongation ε (%)	M. Young E. (MPa)	Tension σ (MPa)
P(MMA-co-BuA)	500	98.55	6.65
P(MMA-co-BuA) OFI-0.05%	507	25.46	2.51
P(MMA-co-BuA) OFI-0.1%	461	14.05	2.62
P(MMA-co-BuA) OFI-0.5%	433	17.53	2.86
P(MMA-co-BuA) OFI-1%	400	16.16	2.78
P(MMA-co-BuA) AV-0.05%	533	23.73	2.43
P(MMA-co-BuA) AV-0.1%	525	12.65	2.56
P(MMA-co-BuA) AV-0.5%	520	10.88	2.07
P(MMA-co-BuA) AV-1%	407	13.10	3.62

3.5 SEM analysis

Figure 3 shows the micrographs of the P(MMA-co-BuA) and NPsAg nanocomposites synthesized with the extracts of OFI and 1% AV. Figure 3a and 3b shows the micrographs of P(MMA-co-BuA) at different magnifications where a homogeneous flat surface and some bright spots can be observed, which may be due to the mechanical deformation produced during fracture with liquid N_2 in the preparation of the sample. In Figure 3c and 3d, the micrographs of the fracture of the P(MMA-co-BuA) OFI nanocomposite are observed, noting that the NPsAg present a homogeneous distribution in the polymer, some "stripes" are also observed in the nanocomposite, and a deformation of the material during fracture [16]. Figure 4e and 4f represents the micrographs of the P(MMA-co-BuA) AV nanocomposite, where a good distribution of the nanoparticles in the polymeric matrix is observed.

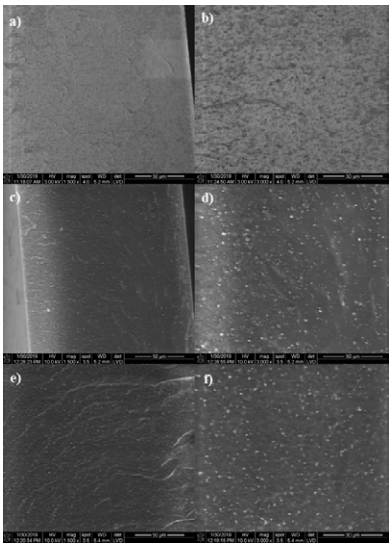

Figure 3. *SEM images a) and b) of the P(MMA-co-BuA) copolymer, c) and d) P(MMA-co-BuA)-OFI-1% nanocomposites and e) and f) P(MMA-co-BuA)-AV-1% nanocomposite obtained by polymerization in emulsion.*

3.6 FTIR analysis

In Figure 4, the FTIR spectra of the nanocomposites are shown in the spectra of the sample without nanoparticles P(MMA-co-BuA) and of the nanocomposites, bands that appear around 2958-2956 cm^{-1} and 2875 cm^{-1} correspond to stretching of methyl CH_3; the 1726 cm^{-1} band represents the stretching of the carbonyl C=O representative of the monomers (MMA/BuA), the 1449 cm^{-1} band represents the bending of the C-CH_2 bond, the 1386 cm^{-1} band represents the OCO stretch, the 1236-1235 cm^{-1} band represents CCO stretch, the 1143 cm^{-1} and 1066-1064 cm^{-1} bands represent asymmetric stretch that occurs from CO, the 841 cm^{-1} band presents the CH_2-CH_2 and finally, at 753 cm^{-1}, the stretching of C-C [16,32,40,48–51] is observed. In general, it is observed that the copolymer and the nanocomposites show similarity in the bands and it can be attributed to the intermolecular

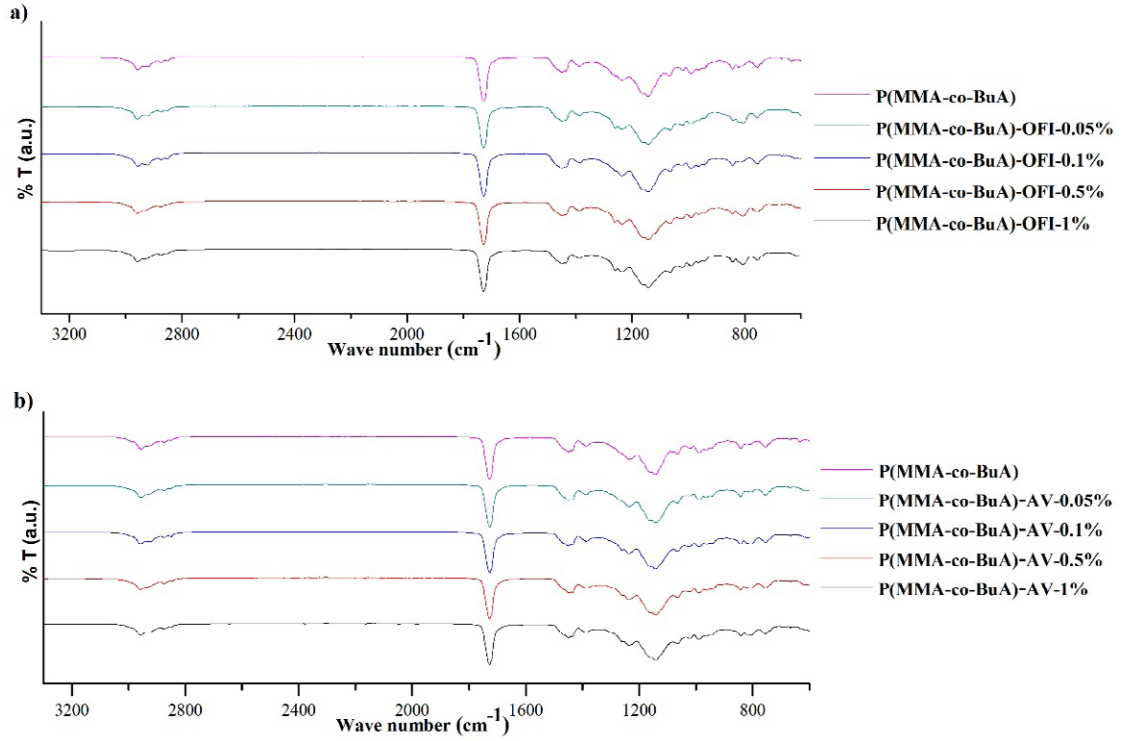

Figure 4. *FTIR spectra a) P(MMA-co-BuA) and NPsAg from the OFI extract and b) P(MMA-co-BuA) and NPsAg from the AV extract at different concentrations.*

interactions between the groups found on the surface of the NPsAg (alcohols, carboxylic acids, ketones and ethers, which come from the extracts of OFI and AV and the groups present in the P(MMA-co-BuA) copolymer, with hydrogen bonding being the most possible interactions. Mamaghani et al. [31] carried out a study where they evaluated the nanocomposites of polymethylmethacrylate-co-butylacrylate-acrylic acid with Ag nanoparticles and observed very similar bands between the spectra and attributed it to intermolecular interactions between the copolymer and the NPsAg.

On the other hand, Scheme 1 shows the interactions of the hydrogen bridge type between the functional groups of the copolymer and the surface groups of the nanoparticles.

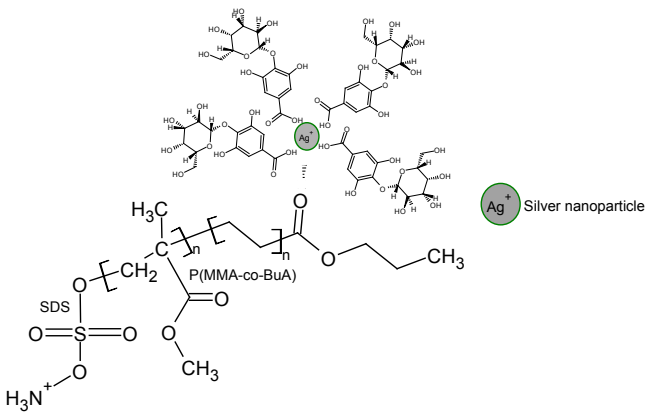

Scheme 1. Schematic representation of P(MMA-co-BuA) with NPsAg.

CONCLUSIONS

The incorporation of NPsAg obtained through green methodologies to the P(MMA-co-BuA) copolymer matrices through in situ emulsion polymerization allowed the synthesis of nanocomposites using sustainable methods and with less environmental impact. Through the FTIR analysis, the interactions that exist between the copolymer and the surface of the nanoparticles can be elucidated. It was possible to observe the surface plasmon resonance (SPR) of the nanocomposites with the NPsAg obtained with both extracts, it was observed in the range of 415- 436 nm. On the other hand, the Tg increases as the concentration of the nanoparticles increases. The results of the mechanical tests indicate that the copolymer without nanoparticles presented greater mechanical resistance and greater elastic behavior with respect to nanocomposites with nanoparticles. Through SEM, it was observed that regardless of the extract used to obtain the nanoparticles, they present good dispersion in the nanocomposite because they are superficially modified.

ACKNOWLEDGEMENT

The authors are grateful for the support of the National Council of Science and Technology (CONACYT) Mexico for the postgraduate scholarship No. 476520 granted to the postgraduate degree in Materials Science and Technology at the Autonomous University of Coahuila.

The authors wish to thank the Faculty of Mechanical and Electrical Engineering of the Autonomous University of Nuevo León and the Center for Innovation, Research and Development in Engineering and Technology (CIIDIT) for providing their facilities, as well as equipment.

NOMENCLATURE

AV	*Aloe vera*
TGA	Thermogravimetric Analysis
BuA	Butylacrylate
DSC	Differential Scanning Calorimetry
FTIR	Fourier-transform infrared spectroscopy
UV-Vis	UV visible spectrophotometry
C	Celsius degrees
g	Grams
MMA	Methyl methacrylate
SEM	Scanning electron microscopy
ml	Milliliters
mm	Millimeters
min	Minutes
NPsAg	Silver nanoparticles
OFI	*Opuntia ficus-indica*
PMMA	Polymethylmethacrylate
P(MMA-co-BuA)	Polymethylmethacrylate-co-butylacrylate
P(MMA-co-BuA)-OFI	Polymethylmethacrylate-co-butylacrylate with silver nanoparticles from the *O. ficus-indica* extract
P(MMA-co-BuA)-AV	Polymethylmethacrylate-co-butylacrylate with silver nanoparticles from the *A. vera* extract
rpm	Revolutions per minute
SPR	Surface plasmon resonance
ε	Elongation at break
σ	Tensile strength
MPa	Megapascal

REFERENCES

1. Ahmad, A. *et al.* Exracellular biosynthesis of silver nanoparticles using the fungus Fusarium oxysporum. *Colloids Surfaces B Biointerfaces* 28, 313–318 (2003).
2. Ahmad, N. *et al.* Biosynthesis of Silver Nanoparticles from Desmodium triflorum: A Novel Approach Towards Weed Utilization. *Biotechnol. Res. Int.* **2011**, 1–8 (2010).
3. Buhin, Z., Blagojevic, S. L. & Leskovac, M. In Situ Emulsion Polymerization and Characterization of Poly(butyl acrylate-co-methyl methacrylate)/Silica Nanosystems. *Polym. Eng. Sci.* 1–7 (2013). doi:10.1002/pen
4. Dong, C. *et al.* Wolfberry fruit (Lycium barbarum) extract mediated novel route for the green synthesis of silver nanoparticles. *Optik (Stuttg).* **130**, 162–170 (2017).
5. Dong, C., Zhang, X., Cai, H. & Cao, C. Green synthesis of biocompatible silver nanoparticles mediated by Osmanthus fragrans extract in aqueous solution. *Optik (Stuttg).* **127**, 10378–10388 (2016).
6. Kouvaris, P. *et al.* Green synthesis and characterization of silver nanoparticles produced using Arbutus Unedo leaf extract. *Mater. Lett.* **76**, 18–20 (2012).
7. Lyutakov, O. *et al.* Silver release and antimicrobial properties of PMMA films doped with silver ions, nano-particles and complexes. *Mater. Sci. Eng. C* **49**, 534–540 (2015).
8. Mo, Y. Y. *et al.* Green synthesis of silver nanoparticles using eucalyptus leaf extract. *Mater. Lett.* **144**, 165–167 (2015).
9. Rivera-rangel, R. D., González-muñoz, M. P., Avila-rodriguez, M., Razo-lazcano, T. A. & Solans, C. Green synthesis of silver nanoparticles in oil-in-water microemulsion and nano-emulsion using geranium leaf aqueous extract as a reducing agent. *Colloids Surfaces A* **536**, 60–67 (2018).
10. Rana, A., Yadav, K. & Jagadevan, S. A comprehensive review on green synthesis of nature-inspired metal nanoparticles: Mechanism, application and toxicity. *J. Clean. Prod.* **272**, 122880 (2020).
11. Allahbakhsh, A. PVC/rice straw/SDBS-modified graphene oxide sustainable Nanocomposites: Melt mixing process and electrical insulation characteristics. *Compos. Part A Appl. Sci. Manuf.* **134**, 105902 (2020).
12. Parida, D. *et al.* Polymer-assisted in-situ thermal reduction of silver precursors: A solventless route for silver nanoparticles-polymer composites. *Chem. Eng. J.* **389**, 123983 (2020).
13. Awad, M. A. *et al.* Greener synthesis, characterization, and antimicrobiological effects of helba silver nanoparticle-PMMA nanocomposite. *Int. J. Polym. Sci.* **2019**, (2019).
14. Siddiqui, N., Bhardwaj, A., Hada, R., Yadav, V. S. & Goyal, D. Synthesis, characterization and antimicrobial study of poly (methyl methacrylate)/Ag nanocomposites. *Vacuum* **153**, 6–11 (2018).
15. Pérez-Martínez, B. T. *et al.* Miniemulsion copolymerization of (meth)acrylates in the presence of functionalized multiwalled carbon nanotubes for reinforced coating applications. *Beilstein J. Nanotechnol.* **8**, 1328–1337 (2017).
16. 1Berber, H., Ucar, E. & Sahinturk, U. Synthesis and properties of waterborne few-layer graphene oxide/poly(MMA-co-BuA) nanocomposites by in situ emulsion polymerization. *Colloids Surfaces A Physicochem. Eng. Asp.* **531**, 56–66 (2017).
17. Bourgeat-Lami, E., Faucheu, J. & Noël, A. Latex routes to graphene-based nanocomposites. *Polym. Chem.* **6**, 5323–5357 (2015).
18. Karakus, S. *et al.* Preparation and characterization of carboxymethyl cellulose/poly (ethylene glycol) -rosin pentaerythritolester polymeric nanoparticles: Role of intrinsic viscosity and surface morphology. *Surfaces and Interfaces* **21**, 100642 (2020).
19. Alghunaim, N. S. In situ synthesis and investigation poly (methyl methacrylate)/polycarbonate nanocomposites incorporated with copper oxide nanoparticles. *Results Phys.* **19**, 103368 (2020).
20. Rodrigues, L. D. A. *et al.* Colloidal properties and cytotoxicity of enzymatically hydrolyzed cationic starch-graft-poly(butyl acrylate-co-methyl methacrylate) latex by surfactant-free emulsion polymerization for paper coating application. *Prog. Org. Coatings* **145**, 105693 (2020).

21. Wang, R. *et al.* Polymer/particle/water intermolecular interaction regulated freeze-dried Pickering emulsion morphology. *Colloids Surfaces A Physicochem. Eng. Asp.* **603**, 125289 (2020).
22. Bakhshi, H., Zohuriaan-Mehr, M. J., Bouhendi, H. & Kabiri, K. Spectral and chemical determination of copolymer composition of poly (butyl acrylate-co-glycidyl methacrylate) from emulsion polymerization. *Polym. Test.* **28**, 730–736 (2009).
23. Gharieh, A., Khoee, S. & Mahdavian, A. R. Emulsion and miniemulsion techniques in preparation of polymer nanoparticles with versatile characteristics. *Adv. Colloid Interface Sci.* **269**, 152–186 (2019).
24. Ghaffari, T., Hamedirad, F. & Ezzati, B. In Vitro Comparison of Compressive and Tensile Strengths ofAcrylic Resins Reinforced by Silver Nanoparticles at 2% and0.2% Concentrations. *J. Dent. Res. Dent. Clin. Dent. Prospects* **8**, 204–209 (2014).
25. Huang, Y., Wang, X., Jin, X. & Wang, T. Study on the PMMA/GO nanocomposites with good thermal stability prepared by in situ Pickering emulsion polymerization. *J. Therm. Anal. Calorim.* **117**, 755–763 (2014).
26. Kuila, T. *et al.* Characterization and properties of in situ emulsion polymerized poly(methyl methacrylate)/graphene nanocomposites. *Compos. Part A Appl. Sci. Manuf.* **42**, 1856–1861 (2011).
27. Lin, Y., Liu, Y., Zhang, D., Chen, C. & Wu, G. Radiation resistance of poly(methyl methacrylate)/reduced graphene oxide nanocomposites fabricated through latex mixing and in situ reduction. *Chem. Eng. J.* **315**, 516–526 (2017).
28. Meng, L., Soucek, M. D., Li, Z. & Miyoshi, T. Investigation of a non-isocyanate urethane functional monomer in latexes by emulsion polymerization. *Polymer (Guildf).* **119**, 83–97 (2017).
29. Salavagione, H. & Martínez, G. Nanocompuestos poliméricos de grafeno: preparación y propiedades. *Rev. Iberoam. Polímeros* **12**, 53–63 (2011).
30. Liu, H. *et al.* In situ visualization and real-time tracking of emulsion and miniemulsion polymerization at the microscale via fluorescence imaging. *Chem. Eng. Sci.* **211**, 115288 (2020).
31. Mamaghani, M. Y., Pishvaei, M. & Kaffashi, B. Synthesis of latex based antibacterial acrylate polymer/nanosilver via in situ miniemulsion polymerization. *Macromol. Res.* **19**, 243–249 (2011).
32. Abdelaziz, M. & Abdelrazek, E. M. Thermal-optical properties of polymethylmethacrylate/silver nitrate films. *J. Electron. Mater.* **42**, 2743–2751 (2013).
33. Vera García, P. F. *et al.* Estudio del comportamiento de diferentes extractos de plantas en la biosíntesis de nanopartículas de plata asistida por microondas. *Afinidad* **592**, 68–78 (2021).
34. Elechiguerra, J. L. *et al.* Corrosion at the nanoscale: The case of silver nanowires and nanoparticles. *Chem. Mater.* **17**, 6042–6052 (2005).
35. Jie, Y., Yonghua, L., Pei, W. & Hai, M. Integral fluorescence enhancement by silver nanoparticles controlled via PMMA matrix. *Opt. Commun.* **284**, 494–497 (2011).
36. Pourmortazavi, S. M., Taghdiri, M., Makari, V. & Rahimi-Nasrabadi, M. Procedure optimization for green synthesis of silver nanoparticles by aqueous extract of Eucalyptus oleosa. *Spectrochim. Acta - Part A Mol. Biomol. Spectrosc.* **136**, 1249–1254 (2015).
37. Lakayan, D. *et al.* Angular scanning and variable wavelength surface plasmon resonance allowing free sensor surface selection for optimum material- and bio-sensing. *Sensors Actuators, B Chem.* **259**, 972–979 (2018).
38. Deshmukh, R. D. & Composto, R. J. Surface segregation and formation of silver nanoparticles created in situ in poly(methyl methacrylate) films. *Chem. Mater.* **19**, 745–754 (2007).
39. Thomas, R. *et al.* Biofabricated silver nanoparticles incorporated polymethyl methacrylate as a dental adhesive material with antibacterial and antibiofilm activity against Streptococcus mutans. *3 Biotech* **8**, 0 (2018).
40. Youssef, A. M., Malhat, F. M., Abdel Hakim, A. A. & Dekany, I. Synthesis and utilization of poly (methylmethacrylate) nanocomposites based on modified montmorillonite. *Arab. J. Chem.* **10**, 631–642 (2017).
41. Ramimoghadam, D., Hussein, M. Z. Bin & Taufiq-Yap, Y. H. The effect of sodium dodecyl sulfate (SDS) and cetyltrimethylammonium bromide (CTAB) on the properties of ZnO synthesized by hydrothermal method. *Int. J. Mol. Sci.* **13**, 13275–13293 (2012).
42. Alsharaeh, E. H. Polystyrene-poly(methyl methacrylate) silver nanocomposites: Significant modification of the thermal and electrical properties by microwave irradiation. *Materials (Basel).* **9**, (2016).
43. Asiri, A. M. Improved Photochromic and Fatigue Performance furylethylidene) -succinicanhydride Doped in Polyurethane Thin Film. *Polym. Eng. Sci.* 1–5 (2011). doi:10.1002/pen
44. Tripathi, S. N., Saini, P., Gupta, D. & Choudhary, V. Electrical and mechanical properties of PMMA/reduced graphene oxide nanocomposites prepared via in situ polymerization. *J. Mater. Sci.* **48**, 6223–6232 (2013).
45. Zhang, L. Y. & Zhang, Y. F. In situ fast polymerization of graphene nanosheets-filled poly(methyl methacrylate) nanocomposites. *J. Appl. Polym. Sci.* **133**, 1–7 (2016).
46. Morimune, S., Nishino, T. & Goto, T. Ecological approach to graphene oxide reinforced Poly (methyl methacrylate) nanocomposites. *ACS Appl. Mater. Interfaces* **4**, 3596–3601 (2012).
47. Monje, A. & Reséndiz, J. R. Síntesis de materiales a base de uretano reforzados con nanopartículas metálicas. I, Síntesis y caracterización. *Rev. Iberoam. polímeros* **14**, 28–38 (2013).
48. Cheng, S., Zhao, Y. & Wu, Y. Surfactant-free hybrid latexes from enzymatically hydrolyzed starch and poly(butyl acrylate-methyl methacrylate) for paper coating. *Prog. Org. Coatings* **118**, 40–47 (2018).
49. Gong, S., Chen, H., Zhou, X. & Gunasekaran, S. Synthesis and applications of MANs/poly(MMA-

co-BA) nanocomposite latex by miniemulsion polymerization. *R. Soc. Open Sci.* **4**, (2017).
50. Navarro, C. H. *et al.* Síntesis y caracterización de un recubrimiento de tipo PMMA-CaO. *Superf. y Vacío* **23**, 31–35 (2010).
51. Shanti, R. *et al.* Poly(methyl methacrylate-co-butyl acrylate-co-acrylic acid): Physico-chemical characterization and targeted dye sensitized solar cell application. *Mater. Des.* **108**, 560–569 (2016).